PROGRESS IN PHOTOVOLTAICS: RESEARCH AND APPLICATIONS, VOL. 5, 29–50 (1997)

Research

Progress in Low-temperature Surface Passivation of Silicon Solar Cells using Remote-plasma Silicon Nitride

Armin G. Aberle* and Rudolf Hezel
Institut für Solarenergieforschung Hameln/Emmerthal (ISFH), D-31860 Emmerthal, Germany

Using a remote-plasma technique as opposed to the conventional direct-plasma technique, significant progress has been obtained at ISFH in the area of low-temperature surface passivation of p-type crystalline silicon solar cells by means of silicon nitride (SiN) films fabricated at 350–400°C in a plasma-enhanced chemical vapour deposition system. If applied to the rear surface of the low-resistivity p-type substrates, the remote-plasma SiN films provide outstanding surface recombination velocities (SRVs) as low as 4 cm s^{-1}, which is by a clear margin the lowest value ever obtained on a low-resistivity p-Si wafer passivated by a solid film, including highest quality thermal oxides. Compared to direct-plasma SiN films or thermally grown oxides, the remote-plasma films not only provide significantly better SRVs on low-resistivity p-silicon wafers, but also an enormously improved stability against ultra-violet (UV) light. The potential of these remote-plasma silicon nitride films for silicon solar cell applications is further increased by the fact that they provide a surface passivation on phosphorus-diffused emitters which is comparable to high-quality thermal oxides. Furthermore, if combined with a thermal oxide and a caesium treatment, the films induce a UV-stable inversion-layer emitter of outstanding electronic quality.

Due to the low deposition temperature and the high refraction index, these remote-plasma SiN films act as highly efficient surface-passivating antireflection coatings. Application of these films to cost-effective silicon solar cell designs presently under development at ISFH turned out to be most successful, as demonstrated by diffused p-n junction cells with efficiencies above 19%, by bifacial p-n junction cells with front and rear efficiencies above 18%, by mask-free evaporated p-n junction cells with efficiencies above 18% and by MIS inversion-layer cells with a new record efficiency of above 17%. All cells are found to be stable during a UV test corresponding to more than 4 years of glass-encapsulated outdoor operation. © 1997 by John Wiley & Sons, Ltd. Progr. Photovolt. 5: 29–50, 1997

(No. of Figures: 19. No. of Tables: 5. No. of Refs: 48.)

* Correspondence to: A. G. Aberle, Institute for Solar Energy Research (ISFH), Am Ohrberg 1, D-31860 Emmerthal, Germany

CCC 1062–7995/97/010029–22$17.50

Received 12 August 1996
Revised 10 September 1996

INTRODUCTION

At ISFH, a research project is under way aiming at the development of cost-effective, industrially feasible 17–20% efficient p-n junction as well as metal–insulator–semiconductor inversion-layer (MIS-IL) solar cells fabricated on large-area single- and multicrystalline p-Si wafers. The cells are made without photolithography, and, as a further common characteristic feature, are surface passivated by low-temperature plasma-enhanced chemical vapour deposition (PECVD) silicon nitride (SiN) films which simultaneously act as very efficient antireflection (AR) coatings. All cell types under investigation are ultimately intended to have a light-sensitive, SiN-passivated rear surface ('bifacial' cell), allowing further significant reductions of the costs of photovoltaic (PV) electricity by exploiting the light reflected from the surroundings onto the rear of the cells. In order to eliminate the need for an additional, costly p^+ diffusion below the rear metal electrode, we only consider p-type wafers that are relatively heavily doped ($\leqslant 2\ \Omega \cdot \mathrm{cm}$).

In recent months, using a remote-plasma technique as opposed to the conventional direct-plasma technique, significant progress has been obtained at ISFH in the area of low-temperature surface passivation of p-type silicon solar cells by means of plasma silicon nitride films. Hence, after a brief discussion of the theoretical impact of surface recombination on the efficiency of silicon solar cells and the technological problems associated with the present standard passivation scheme of silicon solar cells (the high-temperature thermal oxidation), the first half of the paper reports on the passivation properties of remote-plasma SiN films on p-type silicon solar cell substrates and on phosphorus-diffused silicon surfaces. Since the SiN films are intended for use on solar cells, particular attention is paid to the injection-level dependence of the effective surface recombination velocity[1] as well as to the UV stability of the passivation schemes.

In the second half of the paper, the optimized remote-plasma SiN films are applied to three different types of low-temperature passivated silicon solar cells presently under development at ISFH. The first design is a bifacial p-n junction cell using a random-pyramid surface texture and standard shadow mask vacuum evaporation. The second design is a new MIS-IL cell recently proposed by us.[2] This so-called 'truncated-pyramid' cell features a random-pyramid surface texture, shadow mask evaporation and truncated pyramids, leading to improved cell performance. The third design is a p-n junction cell with a mechanically V-grooved front surface, enabling the mask-free formation of the front grid by means of shallow-angle vacuum evaporation. As recently mentioned, this method can enormously reduce the metal consumption and increase the throughput (and hence the economy) of vacuum evaporation.[3] In addition to the standard illuminated I–V measurements, an extended UV test is performed on the cells in order to investigate their UV stability.

It should be noted that, owing to the preliminary status of the research work, the cells presented in this paper are fabricated on $2.5 \times 2.5\ \mathrm{cm}^2$ float-zone (FZ) silicon wafers. Since perimeter recombination is a major loss mechanism in small-area p-n junction cells, the emitter diffusion of the investigated p-n cells is limited to an area of $2.0 \times 2.0\ \mathrm{cm}^2$ by means of a masking thermal oxide or an SiN film. Furthermore, some of the presented truncated-pyramid cells and V-grooved cells have a standard oxide-passivated, point-contacted rear surface involving photolithography and chemical etching. This rear-surface design was selected to reveal as clearly as possible the potential of the new emitter designs of the cells.

IMPACT OF SURFACE RECOMBINATION ON SILICON SOLAR CELL EFFICIENCY

Provided the starting silicon wafers are of a sufficient electronic quality, the main challenge for high efficiencies is the minimization of recombination losses at both cell surfaces. In order to illustrate the importance of surface recombination, Figure 1 shows the calculated dependence of the 1-sun efficiency of a 250-μm thick bifacial p-n junction Si solar cell on the front and rear surface recombination velocity (SRV) parameters $S_{0.\mathrm{front}}$ and $S_{0.\mathrm{back}}$ ($S_0 \equiv \sigma v_{\mathrm{th}} D_{\mathrm{it}}$). It should be noted that these simulations were performed for

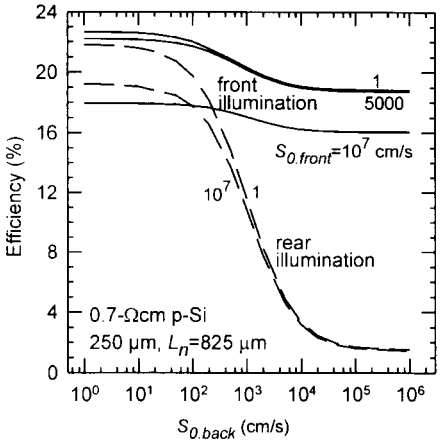

Figure 1. Calculated front-illuminated efficiency (solid lines) and rear-illuminated efficiency (dashed lines) of a bifacial n^+p Si solar cell as a function of the front and rear SRV parameters $S_{0.\mathrm{front}}$ and $S_{0.\mathrm{back}}$ (assumptions: AM1.5G, 300 K, 250 μm thick wafer, 5% reflection at both surfaces, moderate light trapping, 0.7 μm thick n^+ emitter with an exponential profile and $N_s = 3 \times 10^{19}$ cm^{-3})

flatband conditions at the rear surface. Hence, at low-injection conditions, the parameter $S_{0.\mathrm{back}}$ is identical to the effective SRV S_{back} of the rear surface.[4] As indicated in Figure 1, separate simulations were performed for the case of front illumination (i.e. no light onto the rear) and the case of rear illumination (i.e. no light onto the front). The cell parameters assumed for these PC-1D simulations[5] are rather typical for single-crystalline high-efficiency p-n junction Si solar cells. The n-diffused emitter is assumed to have a thickness of 0.7 μm and a surface dopant concentration of 3×10^{19} cm^{-3}, giving a sheet resistance of about 170 $\Omega\square^{-1}$. For a realistic value[6] of 5000 cm s^{-1} for the spatially averaged SRV $S_{0.\mathrm{front}}$, this emitter has a J_{oe} of 40 fA cm^{-2}, resulting in a 1-sun open-circuit voltage (V_{oc}) of about 710 mV. This ensures that, for a realistic rear surface recombination velocity, the modelled cell is dominated by base and rear surface recombination. The chosen electron bulk lifetime of 250 μs (or, equivalently, a diffusion length of 825 μm) in the base is representative for single-crystalline 0.7-Ω · cm p-Si wafers.

As can be seen from Figure 1, for front illumination and a well-passivated emitter, the efficiency is 19% for a non-passivated rear surface and approaches 23% if $S_{0.\mathrm{back}}$ is reduced below 100 cm s^{-1}. In order to achieve the 20% front-efficiency goal, $S_{0.\mathrm{back}}$ must be reduced to values below about 10^3 cm s^{-1}, while $S_{0.\mathrm{front}}$ values of about 5000 cm s^{-1} are sufficient. However, the impact of the rear surface passivation is much stronger if the cell is illuminated from the rear. In this case the efficiency is negligible (<3%) for $S_{0.\mathrm{back}}$ values above 10^4 cm s^{-1}, but it improves enormously with reducing $S_{0.\mathrm{back}}$: for $S_{0.\mathrm{back}} =$ 1000 cm s^{-1} it is 10%, for $S_{0.\mathrm{back}} = 500$ cm s^{-1} it is already 15%, for $S_{0.\mathrm{back}} = 100$ cm s^{-1} it is 20% and for $S_{0.\mathrm{back}} < 10$ cm s^{-1} it even approaches 22% for a well-passivated emitter surface. Since the rear surface of actual bifacial cells has metallized and non-metallized areas, the parameter $S_{0.\mathrm{back}}$ in Figure 1 must be considered as an area-averaged SRV. Since metal-contacted regions are characterized by relatively large S values, the simulations reveal that the SRV in the non-metallized rear surface areas must be well below 100 cm s^{-1} for rear efficiencies above 17% of bifacial Si solar cells.

PROBLEMS OF HIGH-TEMPERATURE OXIDE PASSIVATION

Thermal oxidation at high temperatures (~1000°C) provides excellent surface passivation on phosphorus-diffused Si surfaces as well as on n- and p-type Si wafers.[4,7] However, in spite of its success, there are numerous problems associated with thermally grown Si/SiO_2 interfaces:

(i) High temperatures and relatively long processing times (several hours due to the low oxide growth rate of ~1 nm min^{-1}) are clearly not desirable from cost and throughput considerations.

(ii) High temperatures in combination with contaminated furnace tubes can severely degrade the bulk minority-carrier lifetime, requiring expensive electronic-grade processing gases and time- and energy-consuming furnace cleaning steps.
(iii) The large oxygen content of Czochralski (Cz) silicon wafers is known to lead to oxygen precipitates during lengthy high-temperature ($\sim$1000°C) treatments, which may reduce the bulk minority-carrier lifetime.[8]
(iv) Metal contacts cannot withstand the high oxidation temperatures, so the oxide must be opened by means of photolithography and chemical etching or by means of a laser[9] prior to the formation of the contacts, which strongly affects the costs of the finished cells. Alternatively, a relatively thin oxide could be used so that subsequently deposited screen-printed grid lines can be fired through this oxide. However, this procedure has not yet demonstrated good surface passivation.
(v) The effective SRV S_{eff} at thermally oxidized low-resistivity p-Si surfaces strongly depends on the bulk excess electron concentration Δn.[4,7] At large Δn values ($>10^{14}$ cm^{-3}), which corresponds to V_{oc} conditions of high-efficiency Si solar cells, thermal oxide passivation provides good S_{eff} values around 50 cm s^{-1} on 0.7-$\Omega \cdot$ cm p-Si wafers.[4,7] However, the S_{eff} values increase with reducing Δn to values above 500 cm s^{-1} at Δn values around 10^{13} cm^{-3}.[4] Although this phenomenon leads to high open-circuit voltages, it reduces the fill factor and hence the efficiency of the cell.[1,10] This problem can only be reduced to negligible levels by evaporation of an Al film onto the oxide and a subsequent anneal for about 20 min at 400°C. This so-called 'Alneal' generates atomic hydrogen (formed during the oxidation of Al by residual water in the oxide), effectively reducing the Si/SiO_2 interface state density. Furthermore, owing to work function differences, an Al capping layer increases the band bending at the p-type surface. Thus, the field-effect passivation from the positive fixed oxide charges Q_{f} is strongly enhanced.[4] This technique is exploited at the rear surface of record-efficiency PERL solar cells fabricated on 1–2 $\Omega \cdot$ cm p-Si wafers.[11,12] Obviously, such an Al-covered structure cannot be used for the rear surface of bifacial cells. Furthermore, in the case of monofacial cells, the technique requires contact holes to be opened for the rear electrode, which appears to be a relatively expensive additional processing step.
(vi) The SRV resulting from thermal oxides grown on non-diffused silicon surfaces is not stable against the UV photons of the terrestrial solar spectrum.[13,14]

LOW-TEMPERATURE SURFACE PASSIVATION BY PECVD SiN

Direct-plasma versus remote-plasma technology

In order to eliminate the above problems associated with the high temperatures during the thermal oxidation of silicon, significant effort has been devoted in the past to the development of low-temperature ($\leqslant$400°C) surface passivation schemes. The most successful of these approaches has turned out to be the formation of SiN films by means of the PECVD technique.[15,16] On p-Si wafers best suited for 1-sun applications ($\leqslant 1\ \Omega \cdot$ cm), SRVs around 100 cm s^{-1} have been obtained using PECVD silicon nitride.[17,18] These SiN films were generated in parallel-plate reactors, where the gases (SiH_4, NH_3) are excited by means of an electromagnetic field (frequency 13.56 MHz or in the range 10–500 kHz). A schematic of the parallel-plate PECVD system installed at ISFH is shown in Figure 2(a). It should be noted that at the present point in time most industrially used PECVD systems are based on this particular plasma excitation technology (however, for high-throughput batch processing, the vacuum chamber is replaced by a long furnace tube and the processing gases are injected into one end of this tube). Although the obtained S values of about 100 cm s^{-1} on low-resistivity p-Si wafers are a creditable achievement with regard to the speed of the film deposition (a few minutes) and the low temperatures involved ($\leqslant$400°C), they are not sufficient for rear efficiencies of bifacial Si cells above 17%, as discussed above. Furthermore, as will be shown, SiN films fabricated in parallel-plate PECVD systems cannot maintain the excellent S_{eff} values required for rear efficiencies of 17% if exposed to the UV photons of the terrestrial solar spectrum.

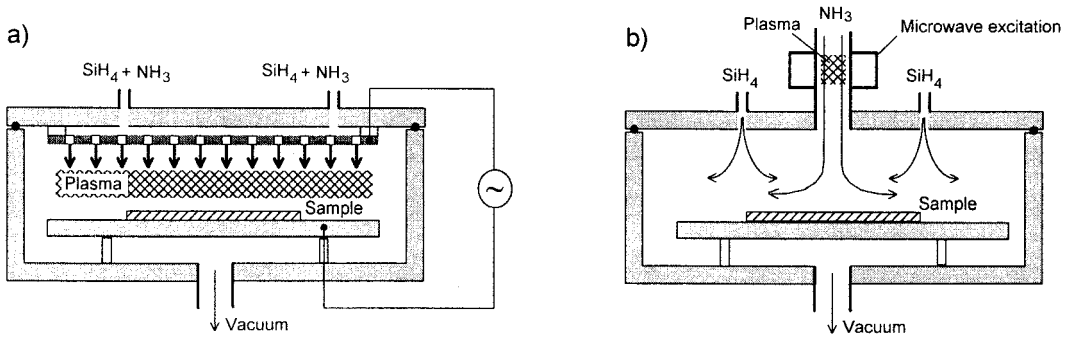

Figure 2. (a) Plasma-enhanced chemical vapour deposition of SiN in a conventional parallel-plate reactor. Note that both processing gases (silane and ammonia) are excited by the electromagnetic field and that the wafer is located within the plasma excitation volume ('direct-plasma' technology). (b) Plasma-enhanced chemical vapour deposition of SiN in a remote-plasma reactor. Note that only ammonia is excited by microwaves and that the wafer is located outside the plasma excitation volume

However, there is scope for improvement since the parallel-plate method is well known to damage the silicon surface during the early stage of the deposition process.[19] This results from the fact that in parallel-plate reactors the wafers are directly exposed to the plasma (see Figure 2(a)), leading to surface damage from energetic ionized plasma constituents. This surface damage leads to UV stability problems of direct-plasma SiN films.[20] In recent months, using an alternative plasma excitation approach (the so-called remote-plasma technique of Figure 2(b)), we succeeded in fabricating plasma SiN films with markedly superior S values and an excellent UV stability. These improvements are attributed to the elimination of the plasma damage to the silicon surface and, possibly, to the fact that only ammonia is excited, leading to a different 'plasma chemistry' in the reaction volume.[21] In the following we will summarize the most important passivation properties of these remote-plasma SiN films. It should be emphasized that plasma SiN films are of an amorphous structure and contain large amounts of hydrogen. Hence, the abbreviation 'SiN' used throughout this work should be interpreted as a-Si_xN_y : H.

Passivation of p-silicon wafers with PECVD SiN films

Figure 3 shows the results from an experiment performed at ISFH on 1.5-Ω · cm Fz p-Si wafers in order to determine the optimum PECVD deposition temperature of the two above-mentioned plasma excitation approaches. The results were obtained from microwave-detected photoconductance decay

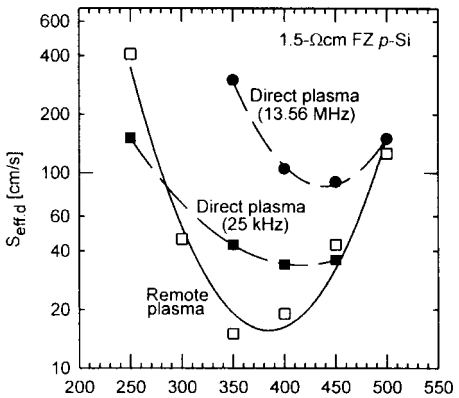

Figure 3. Measured $S_{\text{eff.d}}$ values of single-crystalline 1.5-Ω · cm p-Si wafers passivated at different temperatures by direct-plasma and remote-plasma SiN films

(MW-PCD) measurements after laser pulse excitation.[17,22] The MW-PCD measurements were performed at room temperature, using about 50 mW cm^{-2} of 'white' bias light. Assuming a bulk electron lifetime of 1.7 ms for the investigated 1.5-$\Omega \cdot$ cm FZ p-Si wafers,[23] the differential SRV $S_{\text{eff.d}}$ was calculated from the measured effective minority-carrier lifetime τ_{eff} of the PCD transient.[24,25] As shown in Ref. 25, $S_{\text{eff.d}}$ is sufficient to quantify the electronic performance of an SiN-passivated silicon surface since it typically deviates by less than a factor of 2 from the actual SRV S_{eff} of the surface. The actual SRV S_{eff} is much harder to obtain since its determination requires measurement of the injection-level dependence of $S_{\text{eff.d}}$ over a very large range of injection levels.[25] For this reason we often use the differential quantity $S_{\text{eff.d}}$ instead of the actual SRV S_{eff} in order to quantify the quality of a passivated surface. However, it must always be kept in mind that the actual S_{eff} is the decisive quantity for solar cells. According to Figure 3, for both plasma excitation techniques, optimum surface passivation is obtained if the films are deposited at intermediate temperatures of around 400°C. Another important result is that the remote-plasma SiN films provide $S_{\text{eff.d}}$ values that are significantly better than those of the direct-plasma films. As will be shown below, the remote SiN films furthermore have a much better UV stability than direct-plasma films.

It should be noted that the fabrication of SiN films by means of the PECVD technique involves several processing parameters that can be varied independently over a relatively large parameter range. The most important parameters are the deposition temperature (i.e. the temperature of the silicon wafer), the plasma excitation power, the plasma excitation frequency and the flow rates of the processing gases. Hence, it is obvious that for each particular PECVD system a thorough optimization study must be performed in order to determine the parameter set providing optimum performance. Up to the present point in time, using 'design-of-experiments' methods, we have only performed a comprehensive optimization study for our remote-plasma SiN films.[26,27] The processing parameters giving the best results are: substrate temperature 375°C, pressure 270 mTorr, 50 sccm NH_3, 3 sccm SiH_4, microwave power 60 W. These parameters result in plasma SiN films with a refractive index of about 2.3, indicating a silicon-rich nitride. Since a corresponding complete optimization study has not yet been performed for our direct-plasma films, the direct-plasma results of Figure 3 should be considered as preliminary.

Figure 4 shows the measured actual effective SRVs at polished and textured 1.5-$\Omega \cdot$ cm Fz p-Si surfaces passivated by 375°C remote-plasma SiN films as a function of the bulk excess electron concentration Δn.[23,28] The SRV improves markedly with increasing bulk injection level, approaching values as low as 4 cm s^{-1} for polished surfaces and Δn values around 10^{15} cm^{-3}. This is by a clear margin the lowest SRV that has ever been obtained on a low-resistivity p-Si wafer passivated by a solid film, regardless of the complexity, the speed and the temperature of the film deposition process. Most important for solar cell applications is the experimental result that the introduction of a surface texture (random pyramids) leads

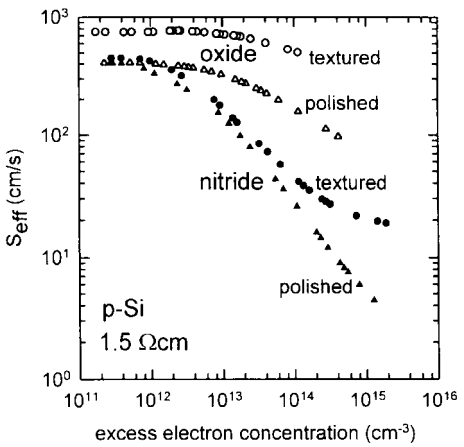

Figure 4. Measured $S_{\text{eff}}(\Delta n)$ dependence at the surfaces of polished and textured 1.5-$\Omega \cdot$ cm p-Si wafers passivated by remote-plasma SiN and thermally grown silicon dioxide

only to a relatively small increase of the SRV. For comparison, the measured dependence of a high-quality thermal oxide grown at ISFH on an identical substrate is included. Clearly, for polished as well as textured surfaces, the SiN film provides far better surface passivation than the thermal oxide. It should be noted that the quality of this oxide is comparable to those grown in other leading silicon solar cell fabrication laboratories, such as the University of New South Wales[29] or the Fraunhofer Institute FhG-ISE.[30]

Passivation of p-silicon wafers with SiO/Cs/SiN schemes

In order to generate a stable inversion-layer emitter with a sufficiently low sheet resistance (<5 kΩ $\square^{-1}$), the ISFH inversion-layer solar cells possess a p-Si/SiO/Cs/SiN passivation scheme. The tunnel oxide of our standard MIS-IL cells is thermally grown at 500°C to a thickness of about 1.5 nm.[31] In order to reduce the emitter sheet resistance, the oxidized wafer is dipped into a CsCl solution prior to the PECVD SiN deposition. Although the incorporation of Cs reduces the surface passivation properties,[32] it is necessary for high fill factors of the cells. Figure 5 shows the measured effective lifetimes of 1.5-$\Omega \cdot$cm p-Si wafers passivated by such SiO/Cs/SiN schemes as a function of the oxidation temperature of the thin thermal oxide.[33] In all experiments the oxidation time was 30 min. An enormous increase of the effective minority-carrier lifetime is achieved by increasing the oxidation temperature. Two possible effects may be responsible for the observed behaviour. First, the oxide and/or the oxide/silicon interface quality may be much better at elevated oxidation temperatures. Second, the oxide thickness increases with increasing oxidation temperature, thus reducing the negative impact of the CsCl dip onto the interface state density.[32]

As suggested by Figure 5, the oxide of the truncated-pyramid cells described below was grown at 800°C to a thickness of about 3 nm. Additional capacitance–voltage measurements revealed that this is still thin enough to get the full benefit from the CsCl dip with regard to the emitter sheet resistance. However, the negative impact on the interface state density is enormously reduced, allowing us to obtain virtually the same effective carrier lifetimes as in the case of the above-mentioned remote-plasma SiN films. This is a decisive prerequisite for the improved inversion-layer cell efficiencies described in the cell results section.

Passivation of phosphorus-diffused emitters with PECVD SiN

As already shown by other research groups,[34,35] PECVD SiN films provide an excellent and UV-stable surface passivation on phosphorus-diffused emitters. The n^+-emitters investigated in Ref. 34 were passivated at 275°C with a 13.56-MHz direct-plasma SiN film, providing emitter saturation current densities J_{oe} of about 220 fA cm^{-2} at 300 K. These SiN-passivated emitters were found to be stable

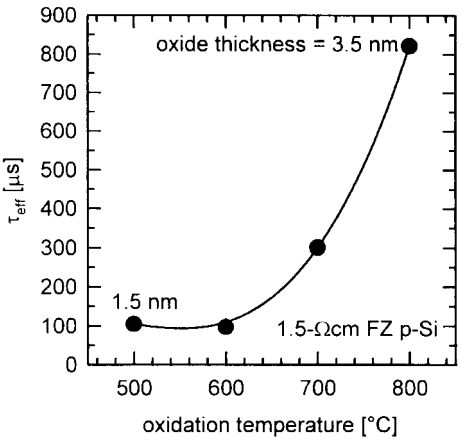

Figure 5. Measured effective lifetimes τ_{eff} of 1.5-$\Omega \cdot$cm FZ p-Si wafers passivated on both sides with a thin oxide grown at different temperatures, a CsCl dip and a 375°C remote-plasma SiN film

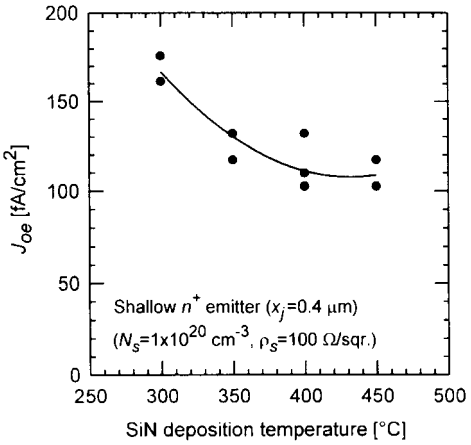

Figure 6. Measured J_{oe} values of remote-plasma SiN-passivated phosphorus-diffused emitters fabricated on shiny etched 1.1-$\Omega \cdot$ cm FZ p-Si wafers as a function of the SiN deposition temperature (300 K, $n_i = 1.0 \times 10^{10}$ cm^{-3})

during a 1000-h exposure to simulated sunlight. Using a similar PECVD system, Ref. 35 reports even lower J_{oe} values of 80 fA cm^{-2} for SiN films deposited at 300°C. Figure 6 summarizes the J_{oe} results from an experiment performed at ISFH on shiny etched 1.1-$\Omega \cdot$ cm FZ p-Si wafers to determine the optimum deposition temperature of remote-plasma SiN films on our standard phosphorus-diffused emitters. The emitters were generated at 830°C using a 20-min deposition step (source: $POCl_3$) and a 20-min drive-in in N_2. Hence, they are relatively shallow ($\sim$0.4 μm) and relatively heavily doped ($N_s \sim 1 \times 10^{20}$ cm^{-3}). The measured emitter sheet resistance is around 100 $\Omega\ \square^{-1}$. According to Figure 6, for SiN deposition temperatures around 400°C the resulting J_{oe} is 110 fA cm^{-2}, indicating that these emitters provide 1-sun open-circuit voltages of up to 687 mV at 300 K. (Note: in Ref. 36 the same data were erroneously analysed with a wafer resistivity of 1.5 $\Omega \cdot$ cm, leading to J_{oe} values being overestimated by 36%.) Owing to their thinness, these emitters exhibit good quantum efficiencies for 'blue' light, resulting in high short-circuit currents of the finished cells.

ULTRAVIOLET STABILITY OF PECVD SiN SURFACE PASSIVATIONS

Since the above-mentioned passivation schemes are intended for use on solar cells, they must be sufficiently stable against the UV photons of the terrestrial solar spectrum in order to ensure the required long-term stability (>20 years) of the corresponding solar cells. Hence, the passivated wafers were illuminated by a 400-W metal halide UV lamp (Hoehnle 400F) and the effective surface recombination velocity was measured by means of the MW-PCD method.[37] Since the terrestrial solar spectrum contains virtually no photons with wavelengths below 320 nm, such photons were eliminated from the spectrum of the UV lamp by means of a UV filter with a cut-off wavelength of 320 nm. As will be shown below, photons with wavelengths above 400 nm do not have any impact on the passivation quality of SiN-passivated silicon wafers. In the wavelength range 320–400 nm, the averaged intensity of the UV lamp used is 7.5 times the intensity of the AM1.5G spectrum. For the corresponding yearly illumination of a PV module we assume 1000 h year^{-1} of AM1.5G radiation, which is rather typical for Germany. The cell temperature was about 60°C during the UV exposure.

All investigated samples are high-quality (100)-oriented boron-doped FZ Si wafers with a resistivity of 1–2 $\Omega \cdot$ cm and a thickness of 300 μm. Prior to the application of identical passivation schemes on both surfaces, the wafers received a standard RCA clean. Samples with SiO/Cs/SiN passivation schemes were oxidized at 800°C. The MW-PCD measurements were performed under a bias light intensity of about 50 mW cm^{-2} at room temperature. For analysis of the effective minority-carrier lifetime τ_{eff} of the measured PCD transient, a bulk electron lifetime of 1.7 ms was assumed, as discussed in Ref. 23.

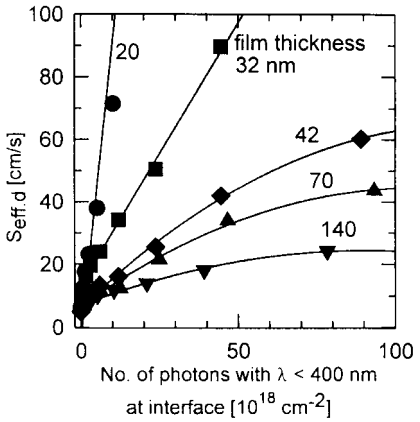

Figure 7. Measured differential SRV $S_{\text{eff.d}}$ of remote-plasma SiN-passivated p-Si wafers as a function of the number of the UV photons reaching the Si/SiN interface and the film thickness (UV cut-off wavelength 320 nm, total UV exposure 120 h)

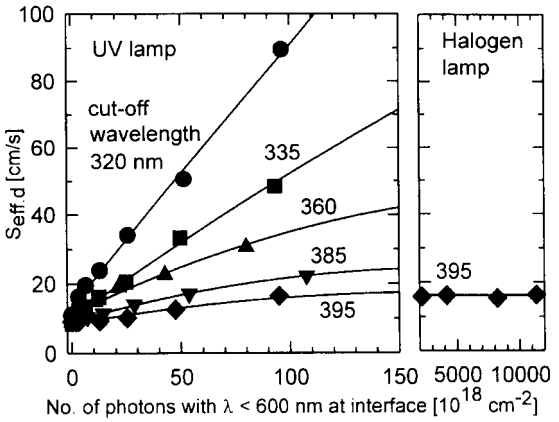

Figure 8. Measured differential SRV $S_{\text{eff.d}}$ of p-Si/SiN passivations as a function of the number of the UV photons reaching the Si/SiN interface and the UV cut-off wavelength (total UV lamp exposure 120 h, film thickness 35 nm)

Differences in the τ_{eff} values of the various samples prior to the UV test are exclusively related to surface passivation effects, since we observe no variation of the bulk minority-carrier lifetime during all processing steps. The same conclusion holds for the UV test itself, since such photons do not modify the bulk minority-carrier lifetime of FZ silicon. (Note that this conclusion would not necessarily apply to solar-grade Cz-silicon.)

Remote-plasma SiN passivations on p-silicon wafers: impact of the film thickness

Figure 7 shows the measured impact of the thickness of the passivating remote-plasma SiN film on the UV stability of 1.5-$\Omega \cdot$ cm p-Si wafers. For this experiment a set of samples with different film thicknesses was illuminated for up to 120 h on each surface, corresponding to about 1 year of non-encapsulated outdoor operation. To eliminate effects from different reflection and absorption properties of the SiN films, $S_{\text{eff.d}}$ is plotted versus the total number of UV photons reaching the Si/SiN interface. It can be seen that the passivation properties of thin (<30 nm) SiN films deteriorate quickly during UV exposure. However, with increasing film thickness the UV stability increases enormously. From Figure 7 it can be concluded that remote-plasma SiN passivations of p-Si solar cell substrates must be relatively thick ($\geqslant 70$ nm) to ensure a sufficient long-term stability.

Remote-plasma SiN passivations on p-Si wafers: impact of the photon wavelength

Figure 8 shows the wavelength dependence of the UV degradation. A set of identical remote-plasma SiN passivated wafers was illuminated using different UV cut-off filters. Samples with relatively thin SiN films (35 nm) were investigated in order to obtain clear effects within reasonable times. It can be seen that the UV stability improves enormously with increasing UV cut-off wavelength. For wavelengths greater than about 400 nm no UV degradation is detectable, in spite of the extreme sensitivity of these test samples with regard to changes in the SRV. To verify this result for much higher photon fluxes, an additional test was performed using a 250-W halogen lamp and a 395-nm cut-off filter. As can be seen in Figure 8, the films are stable under the halogen lamp (3.7 suns, 400 h).

Passivation schemes as used on ISFH silicon solar cells

In Figure 9, the UV stability of a 70-nm thick remote-plasma SiN film as used for the rear surface passivation of our bifacial cells is compared with that of an SiO/Cs/SiN passivation scheme as used on the

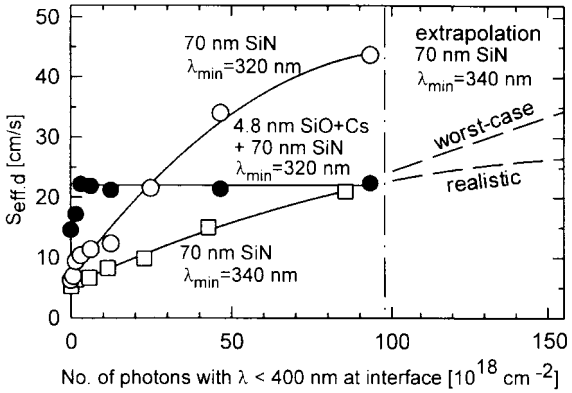

Figure 9. Measured differential SRV $S_{\text{eff.d}}$ of p-Si wafers passivated with remote-plasma SiN films or SiO/Cs/SiN passivation schemes versus the number of UV photons reaching the silicon/insulator interface. Ultraviolet exposure is performed for up to 120 h using 320-nm and 340-nm UV cut-off filters, respectively

front surface of our truncated-pyramid MIS-IL solar cells. The samples are illuminated for up to 120 h on both surfaces using a 320-nm cut-off filter. The behaviour of the 70-nm thick SiN film has already been discussed above. Figure 9 reveals that the SiO/Cs/SiN passivation scheme is stable at an excellently low differential $S_{\text{eff.d}}$ value of 23 cm s^{-1}. Hence, as will be confirmed in the cell results section, the correspondingly fabricated MIS-IL cells are also stable under UV illumination. Furthermore, if applied to the rear surface, this passivation scheme has the potential to achieve stable rear efficiencies of about 20% (see Figure 1).

For the remote-plasma SiN passivation, an additional UV test using a 340-nm cut-off filter was performed in order to simulate the effect from the PV module encapsulation. (Note that standard glass is impenetrable for $\lambda < 340$ nm.) The 120 h of UV exposure on both surfaces correspond to about 2 years of outdoor operation of rear module surfaces. As can be seen, after this time the SiN film still provides excellently low differential $S_{\text{eff.d}}$ values of 20 cm s^{-1}. A linear extrapolation as a worst-case scenario (since the measured $S_{\text{eff.d}}$ curve shows a negative curvature) gives a differential $S_{\text{eff.d}}$ of about 80 cm s^{-1} after 10 years of outdoor operation. Together with Figure 1 this implies that 70-nm thick remote-plasma SiN passivations provide stable 17–18% rear efficiencies of glass-encapsulated bifacial silicon solar cells.

Comparison of the UV stability of remote-plasma and direct-plasma SiN films

Figure 10 shows the measured effective minority-carrier lifetimes of eight representative PCD samples fabricated on 1.5-Ω · cm FZ p-Si wafers as a function of duration of UV exposure.[38] The samples were illuminated for up to 120 h on both surfaces using a 315-nm cut-off filter. Plot (a) shows the case of SiN- or silicon oxide-passivated p-Si wafers, whereas plot (b) shows the results of SiN passivation of phosphorus-diffused or induced-junction emitters fabricated on the same substrates.

According to Figure 10(a), remote-plasma SiN films provide much higher starting lifetimes than direct-plasma SiN films (more than 1 ms as opposed to less than 300 μs). Furthermore, the remote-plasma films exhibit an excellent UV stability compared to our direct-plasma SiN films (both 13.56-MHz high-frequency excitation and 25-kHz low-frequency excitation). Considering Figure 9 and Figure 1, it is clear that additional steps (such as inclusion of UV absorbers into the PV module encapsulation) must be undertaken if our direct-plasma SiN films are used to passivate the rear surface of p-type bifacial silicon solar cells. As discussed above (Figure 9), this is not the case for our remote-plasma SiN films. Also included in Figure 10(a) are two samples passivated by a 105-nm thick high-quality thermal oxide grown at 1050°C. It can be seen that the lifetime of these samples degrades quickly during the first 20 h of UV exposure and then enters a regime where it is only very weakly affected by the UV photons. This result is

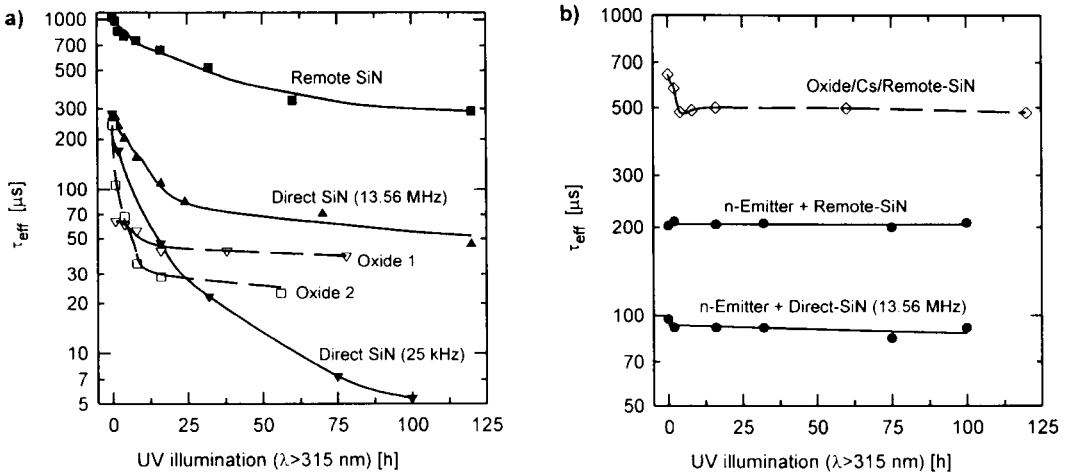

Figure 10. Measured effective minority-carrier lifetimes of eight representative PCD samples versus the duration of the UV exposure. Plot (a) shows the case of silicon nitride- or silicon oxide-passivated 1.5-Ω · cm FZ p-Si wafers, whereas plot (b) shows the results of SiN passivation of phosphorus-diffused or induced-junction emitters fabricated on the same substrates (SiN thickness 70 nm, 300 μm thick shiny etched wafers, UV cut-off wavelength 315 nm, UV exposure of 120 h corresponds to about 1 year of non-encapsulated outdoor operation)

in agreement with References 13 and 14, where it is shown that SiO_2 films thermally grown on non-diffused silicon surfaces cannot maintain very low SRVs under illumination.

In order to investigate the UV behaviour of our SiN-passivated n-diffused emitters, remote-plasma and direct-plasma (13.56 MHz) SiN films were deposited at 400°C. The emitters were generated in the same way as described above (see discussion of Figure 6). In agreement with the results of Ref. 34 we find that PECVD SiN passivation of phosphorus-diffused emitters is stable under UV exposure (see Figure 10(b)). Interestingly, for our present emitter profile, the remote-plasma SiN films provide τ_{eff} values which are about twice as high as those of direct-plasma SiN-passivated emitters. However, these results should be considered as preliminary since we have not yet performed a comprehensive optimization study of our PECVD SiN films on phosphorus-diffused emitters.

The upper curve in Figure 10(b) shows the behaviour of an induced-junction emitter generated by the SiO/Cs/SiN passivation scheme described above. This sample exhibits the same excellent UV stability as the phosphorus-diffused emitters, but at significantly superior effective lifetimes of about 500 μs. This is a clear indication that our induced-junction emitters have the potential to outperform conventional phosphorus-diffused emitters of silicon solar cells.

CELL RESULTS

Bifacial n^+p cells

Application of the above-mentioned low-temperature remote-plasma SiN films to cost-effective p-n junction as well as MIS inversion-layer silicon solar cell designs presently under development at ISFH turned out to be very successful. As an example, Figure 11 shows a schematic of a very simple bifacial p-n junction cell.[39] For simplicity and hence cost effectiveness of the fabrication process, the front and rear metal grids are evaporated through a metal shadow mask prior to deposition of the passivating SiN films on both surfaces, as introduced in Ref. 40. In order to minimize recombination losses at the rear metal grid lines, the cells receive a local Al back surface field (BSF) formed during a 30-min alloying step at 850°C in N_2. Both cell surfaces are textured with random pyramids for reduced reflection losses.

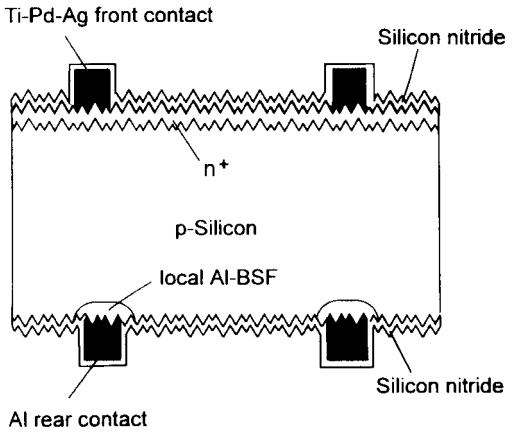

Figure 11. Low-temperature SiN-passivated bifacial p-n junction Si solar cell developed at ISFH

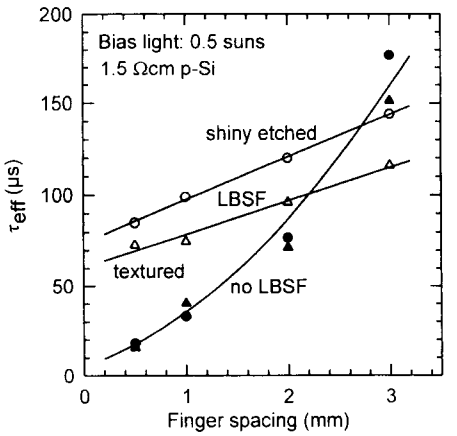

Figure 12. Measured effective electron lifetimes τ_{eff} of Al grid-covered, SiN-passivated, shiny-etched and textured 1.5-$\Omega \cdot$ cm FZ p-Si wafers as a function of the Al grid finger spacing (circles = shiny etched surfaces; triangles = textured surfaces; LBSF = local BSF). The lines are guides to the eye. The surface coverage of each metal grid is around 6%

Figure 12 shows the measured impact of the alloyed local Al BSF and the spacing of the rear Al fingers on the effective electron lifetime of textured and non-textured SiN-passivated 1.5-$\Omega \cdot$ cm FZ p-Si wafers. These results were obtained from MW-PCD measurements using about half a sun of white bias light.[28] The electron diffusion length of the starting material was about 2 mm. For the samples without a local BSF, the recombination losses occur predominantly at the metal contacts. Hence, τ_{eff} increases strongly with increasing finger spacing and does not differ significantly for textured and polished surfaces. A detailed discussion of this dependence can be found in Ref. 28. According to Figure 12, the situation changes significantly if a local BSF is included below the Al grid lines for reduced metal contact recombination. First, for small finger spacings around 0.5 mm, τ_{eff} is about four times higher than for the samples without a local BSF. Second, recombination losses in the non-metallized surface regions are relatively more important, causing τ_{eff} to improve with a smaller slope with increasing finger spacing and also to be lower for textured surfaces than for polished surfaces, as expected from the increased surface area. Interestingly, for large finger spacings ($\geqslant 3$ mm), the cells with a local BSF have lower τ_{eff} values than those without. This indicates that the 850°C alloying step has some negative impact on the uncovered surface areas between the Al grid lines (for instance, by means of evaporation of Al). Hence, the subsequent passivation of the surface by remote-plasma SiN is slightly less effective than for the samples that did not receive the alloying step. As a result of these different trends, the τ_{eff} curves of samples with and without a local BSF cross each other at a finger spacing of about 2.5 mm.

At first sight the results of Figure 12 imply that optimum solar cell performance is obtained for very large finger spacings (>3 mm) and no local BSF below the Al grid lines. However, when applying these results to solar cells, it is important to recall that MW-PCD measurements are performed according to open-circuit conditions of solar cells. Hence, the method is obviously insensitive to resistive effects in the cell and a trade-off between the surface passivation properties and the resistive properties has to be found. Due to the fill factor effect it is obvious that very large finger spacings (>3 mm) will not lead to optimum solar cell efficiency. Furthermore, if the sample contains high-recombination areas (such as metal contacts) that are separated from each other by a distance comparable to or greater than the bulk minority carrier diffusion length, then the actual recombination losses depend critically on the supply of minority carriers to these areas. The samples investigated in this work are operated in low-injection conditions, so that the minority carriers flow predominantly by diffusion along the minority-carrier

Table I. Measured front-illuminated and rear-illuminated 1-sun performance parameters of bifacial n^+p silicon solar cells with and without a local Al-BSF (AM1.5G, 100 mW cm^{-2}, 25°C, aperture area 3.9 cm^2, 200 μm thick 1.5-Ω · cm wafers, both surfaces textured, rear finger spacing 2 mm, measurements performed at ISFH)

Cell type	With local BSF		Without local BSF	
Illumination mode	Front	Rear	Front	Rear
J_{sc} (mA cm^{-2})	35.7	35.0	34.8	31.5
V_{oc} (mV)	639	639	635	632
Fill factor (%)	80.0	79.8	79.9	80.0
Efficiency (%)	18.2	17.8	17.7	15.9

Table II. Measured front- and rear-illuminated 1-sun parameters of SiN-passivated bifacial n^+p silicon solar cells fabricated at ISFH on FZ p-Si wafers (AM1.5G, 100 mW cm^{-2}, 25°C, aperture area 4.0 cm^2, both cell surfaces passivated with 375°C remote SiN, both electrodes evaporated through a metal shadow mask, both cells with local Al-BSF and 2 mm finger spacing on the rear)

Cell	PN1		PN2	
Substrate	1.5 Ω · cm, 200 μm		0.5 Ω · cm, 300 μm	
Surface texture				
Front	Random pyramids		Random pyramids	
Rear	Random pyramids		Non-textured	
Illumination mode	Front	Rear	Front	Rear
J_{sc} (mA cm^{-2})	36.0	35.4	36.7	31.4
V_{oc} (mV)	643	643	647	646
Fill factor (%)	79.6	79.5	81.8	81.2
Efficiency (%)	18.4[a]	18.1[a]	19.4[a]	16.5[a]

[a]Independently confirmed by the Fraunhofer Institute FhG-ISE.[48]

concentration gradient. Since the minority-carrier concentration profile in solar cells depends critically on the operating condition, care must be taken when using MW-PCD results to predict the short-circuit current potential of the cells.

Table I shows the measured front-illuminated and rear-illuminated output characteristics of bifacial n^+p cells with and without a local Al-BSF. The finger spacing of both cells is 2 mm. The cell with a local Al-BSF has a rear efficiency of 17.8%, which is a remarkable 1.9% (absolute) higher than the rear efficiency of the cell without a BSF. This is mainly due to the 11% higher rear short-circuit current in comparison to the cell without a local BSF. The reduced rear-illuminated J_{sc} of the cell without a local BSF is a result of the fact that in this illumination mode a large number of charge carriers are generated in the vicinity of the rear metal contacts. Hence, under short-circuit conditions, the device is extremely sensitive to enhanced rear contact recombination losses. With increasing cell voltage the charge carrier concentrations throughout the cell change strongly, causing recombination losses in other cell areas to become relatively more important. Thus, in spite of the strongly differing J_{sc} values, the rear-illuminated open-circuit voltage of both cell types differs by only about 1%. This J_{sc} effect, which would not have been expected from Figure 12, is a nice demonstration of the above-mentioned remark that care must be taken when using MW-PCD results to predict the short-circuit current potential of solar cells. As predicted by PC-1D (see Figure 1), the influence of the different S_{back} values on the front efficiency is not very strong, with 0.5% (absolute) difference between the two cells.

The best cells of this bifacial type fabricated as yet at ISFH were sent to the Fraunhofer Institute FhG-ISE in order to obtain independently confirmed performance parameters. The corresponding results

are summarized in Table II.[39] The intention behind cell PN1 was to fabricate a 'symmetrical' bifacial cell with identical efficiency under front and rear illumination. Such cells are of interest for applications where a similar amount of light falls onto both cell surfaces. Typical examples are the roof tile concentrator presently under development at the University of New South Wales,[41] the recently developed ISFH compound parabolic concentrator[42] or photovoltaic sound barriers with north-south orientation.[43] For optimum rear efficiency, this cell was fabricated on a 200-μm thick 1.5-Ω · cm FZ p-Si wafer textured on both surfaces. As can be seen from Table II, the goal of a 'symmetrical' cell efficiency has essentially been achieved with a front efficiency of 18.4% and a rear efficiency of 18.1% (i.e. a symmetry factor of above 98%). This is a remarkable result with regard to the simple processing sequence of the cell. The outstanding rear surface passivation provided by the 375°C remote-plasma SiN film leads to the excellent rear efficiency of 18.1%, which is by far the highest value reported to date for a bifacial Si cell with a non-diffused rear surface.

As can be seen from cell PN2, the front efficiency of this cell design can be further improved to 19.4% if the cell is fabricated on a 300-μm thick 0.5-Ω · cm wafer with a non-textured rear surface. This independently confirmed front efficiency is considered to be the highest reported to date for any low-temperature passivated bifacial Si solar cell. The increased wafer thickness and doping level as well as the non-textured rear surface lead to a 1.6% (absolute) reduction of the rear efficiency. These cells are ideally suited for typical bifacial cell applications (i.e. installation in front of a white wall)[44] where the light intensity at the rear surface of the PV module is below about 50% of the front intensity. In such applications, owing to their superior front efficiency, these cells produce more electricity than the above-mentioned symmetrical devices.

Truncated-pyramid MIS-IL cells

The second cell structure investigated in this work is a truncated-pyramid MIS-IL cell.[2,33] Compared to our standard MIS-IL cells,[31] the fabrication sequence is modified in order to permit fabrication of the SiO/Cs/SiN passivation scheme prior to the formation of the MIS tunnel contact without the use of photolithography. Thus, the temperature restriction during the deposition of the SiN film is eliminated and the optimized SiO/Cs/SiN passivation scheme of Figure 5 (i.e. a thermal oxidation at 800°C, a CsCl dip and a 375°C remote-plasma SiN deposition) can be exploited. This leads to significant improvements of the open-circuit voltage. Table III summarizes the processing sequence of the best truncated-pyramid MIS-IL cell fabricated as yet, while Figure 13 shows a schematic representation of the cell design. The name for this cell type results from processing step 9, where the tips of the randomly distributed pyramids

Table III. Processing sequence of truncated-pyramid MIS-IL silicon solar cells with oxide-passivated rear surface

Step	Process
1	Chemical cleaning
2	Growth of a 200-nm thermal oxide (1050°C, 6 h)
3	Removal of the oxide on the front surface
4	Chemical texturing of the front surface with random pyramids
5	Fabrication of holes in the rear passivating oxide
6	Growth of a 3.5-nm thermal oxide (800°C, 30 min)
7	CsCl dip
8	Remote PECVD deposition of SiN onto front surface (25 nm, 375°C, ~0.5 min)
9	Opening of the front contact areas by means of chemical–mechanical polishing
10	Chemical cleaning
11	Vacuum evaporation of ~5 μm Al onto the rear surface
12	Growth of a 1.5-nm thermal oxide on the truncated pyramids (500°C, 10 min)
13	Vacuum evaporation of ~10 μm Al onto front surface through metal shadow mask
14	Passivation of opened areas between the front grid lines with plasma SiN (60 nm, 250°C, ~1 min)

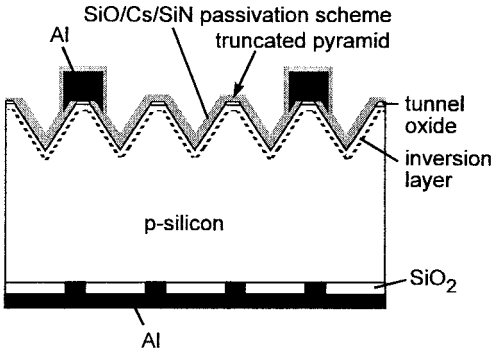

Figure 13. Schematic representation of a truncated-pyramid inversion-layer silicon solar cell

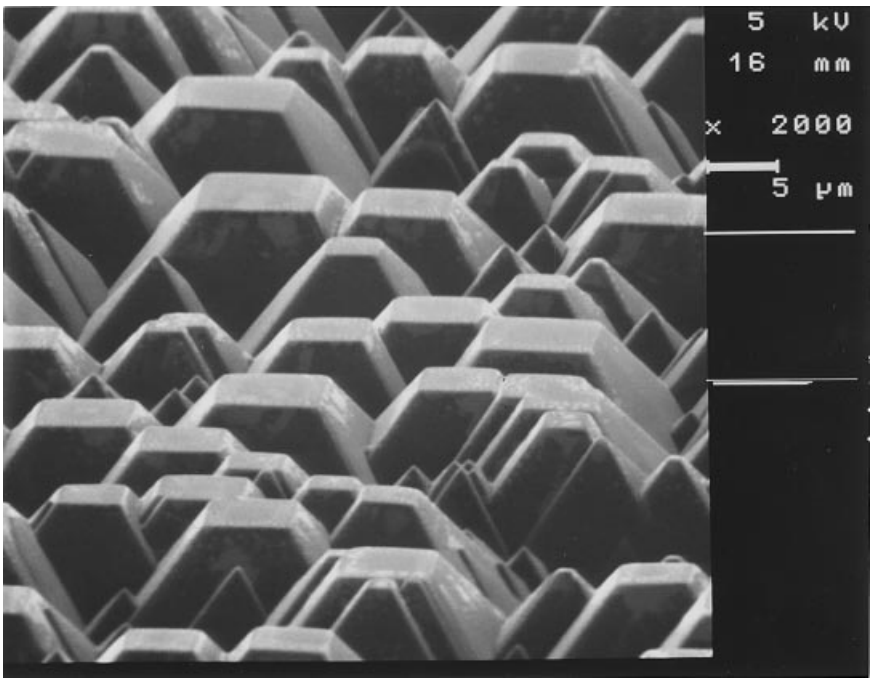

Figure 14. Scanning electron micrograph of non-metallized truncated pyramids on the top surface of a truncated-pyramid solar cell. The passivation layer was removed to improve the quality of the picture

are removed by a gentle chemical–mechanical polishing step, forming truncated pyramids as shown in the scanning electron micrograph of Figure 14.

The open-circuit voltage and the efficiency of our textured standard MIS-IL cells are around 595 mV and 15.7% under standard testing conditions, respectively.[45] As can be seen from Table IV, the truncated-pyramid concept allowed us to improve the open-circuit voltage by more than 40 mV. As a result of the improved V_{oc}, the truncated-pyramid MIS-IL cell has an independently confirmed efficiency of 17.1%, which is a clear improvement over the efficiency of our standard MIS-IL cells. The efficiency of the truncated-pyramid cell reduces only marginally to 16.7% if the cost-effective bifacial rear surface design of Figure 11 is implemented.[33] It should be noted that we also fabricated standard MIS-IL cells with an oxide-passivated, point-contacted rear surface. As expected from the poor emitter properties, this had no effect on the open-circuit voltage of the cells. Hence, the V_{oc} boost of over 40 mV of the truncated-pyramid cells is exclusively due to improved emitter properties.

Table IV. Measured 1-sun parameters of a truncated-pyramid MIS-IL silicon solar cell fabricated at ISFH on a 300-μm thick 0.5-Ω · cm FZ p-Si wafer (AM1.5G, 100 mW cm^{-2}, 25°C, aperture area 4.0 cm^2)

Surface texture	
Front	Random pyramids
Rear	Shiny etched
Electrodes	
Front	Al (shadow mask, perpendicular evaporation)
Rear	Al point contacts (perpendicular evaporation)
J_{sc} (mA cm^{-2})	35.5
V_{oc} (mV)	639
Fill factor (%)	75.5
Efficiency (%)	17.1[a]

[a]Independently confirmed by the Fraunhofer Institute FhG-ISE.[48]

Table V. Measured 1-sun parameters of mechanically V-groove textured MIS-contacted n^+p cells fabricated at ISFH on 400-μm thick 0.5-Ω · cm Fz p-Si wafers. The front surfaces of both cells are passivated by remote-plasma SiN, while at the rear surface a thermally grown oxide in conjunction with Al point contacts is used (AM1.5G, 100 mW cm^{-2}, 25°C, aperture area 4.0 cm^2)

Cell	MIS1	MIS2
Metallization technique	Shadow mask evaporation	Mask-free shallow-angle evaporation
Evaporation angle (°)	~90	~10
J_{sc} (mA cm^{-2})	38.2	36.2
V_{oc} (mV)	652	654
Fill factor (%)	78.4	78.4
Efficiency (%)	19.5	18.6[a]

[a]Independently confirmed by the Fraunhofer Institute FhG-ISE.[48]

Mechanically textured cells with self-aligned metallization

Another interesting cell design utilizing the low-temperature SiN passivation is the MIS-contacted diffused p-n junction cell MIS1 of Table V.[46] The characteristic features of this cell are a mechanically V-grooved front surface (which provides excellent reflection properties) and an MIS tunnel contact formed by perpendicular evaporation of Al through a shadow mask onto a thin (~1.5 nm) thermal oxide. This Al-based MIS contact design has recently been introduced in Ref. 47. Hence, the front and rear electrodes both consist exclusively of Al, which is an interesting aspect with regard to the cost of the cells. The final processing step is the deposition of a remote-plasma SiN film onto the front surface at a slightly reduced temperature of 300°C in order not to degrade the properties of the MIS contact. The excellent reflection and surface passivation properties provide short-circuit currents of 38.2 mA cm^{-2}. Such high currents have previously only been obtained using highest-quality thermal oxides on textured surfaces. Although this cell suffers from a less-than-ideal fill factor, the high J_{sc} ensures that the efficiency exceeds 19%.

Cell MIS2 is similar to cell MIS1 but the front electrode has been obliquely evaporated at an angle of about 10° without the use of a metal shadow mask.[46] This has been possible due to the shading effect of the ridge tops formed by the V-grooved surface texture (see Figure 15). This metallization technique is a decisive prerequisite for an innovative cell concept recently proposed by us, the so-called 'abrased ridge top' (ART) cell.[3] Although J_{sc} of cell MIS2 is smaller than for cell MIS1 (due to excessive metal coverage of the top surface), the achieved efficiency of 18.6% is a clear indication that the mask-free shallow-angle

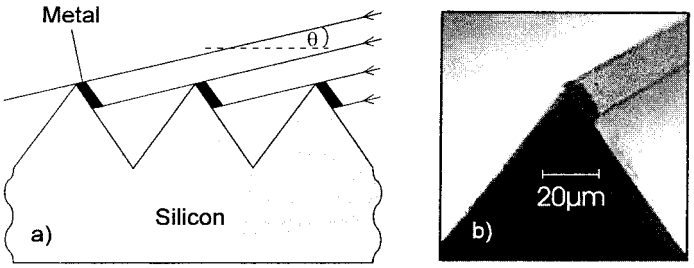

Figure 15. (a) Principle of self-alignment during oblique metal evaporation. (b) Scanning electron-micrograph of an obliquely metallized ridge top

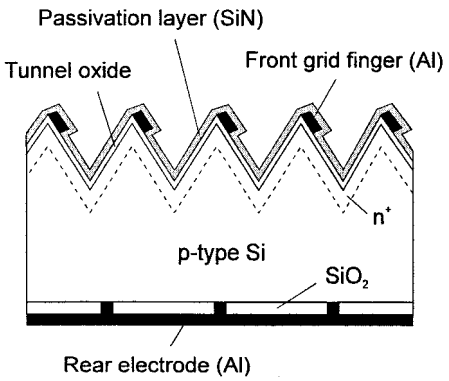

Figure 16. Schematic representation of the MIS-contacted diffused p-n junction cell MIS2 with mechanically grooved, mask-free metallized and low-temperature-passivated front surface

evaporation is a very promising technique for the cost-effective fabrication of the front grid of mechanically structured high-efficiency Si solar cells. Figure 16 shows a schematic representation of cell MIS2.

ULTRAVIOLET STABILITY OF PLASMA SiN-PASSIVATED SILICON SOLAR CELLS

Considering their simple fabrication process, the above-mentioned silicon solar cells exhibit very high efficiencies. These efficiencies are to a large extent the result of an excellent surface passivation by means of remote-plasma PECVD SiN films. An important prerequisite for the required long-term stability of the efficiency of the cells is that the surface passivation quality does not degrade under extended exposure to sunlight. The primary concern in this area is the degradation due to the UV photons in the terrestrial solar spectrum.

It is important to recall that the SiN films of this work are used in two independent ways: passivation of n^+-diffused emitters of p-n junction silicon solar cells; and passivation of the 'pure' (i.e. non-diffused) p-type silicon substrate, e.g. at the front surface of MIS-IL solar cells or at the rear surface of both p-n junction as well as MIS-IL solar cells. In the former case UV stability is not a critical problem since the emitter doping profile reduces the SRV at the SiN/Si interface to a much lower effective SRV at the edge of the space charge region.[4] The UV stability is much more important, however, if SiN is used in the latter case to passivate the non-diffused surfaces of silicon solar cells. In these applications the SiN must directly provide excellent S_{eff} values, which have to be stable under UV exposure since an increase directly affects the surface passivation. This problem is already known from the Stanford concentrator Si solar cells,

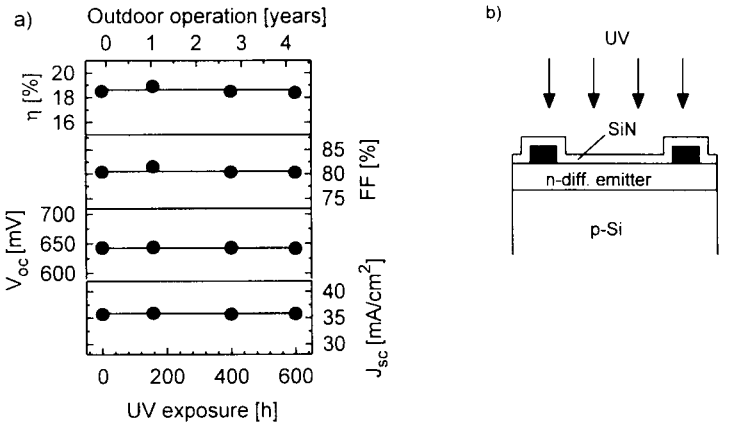

Figure 17. (a) Measured parameters of a remote-plasma SiN-passivated diffused p-n junction Si solar cells during UV exposure. The solid lines are first-order regressions. (b) Schematic of the illuminated front surface design

where a front surface passivation by a thermal oxide without a diffused surface region is not stable under concentrated sunlight.[13,14]

The UV stability was tested for four different ISFH silicon solar cell structures passivated by remote-plasma SiN films or by SiO/Cs/remote-plasma SiN schemes. The first three cell structures are those described in the previous section on cell results. The UV test was performed on the front surface of an 18.5% efficient p-n junction cell, on the rear surface of a bifacial p-n junction cell with 17.2% rear efficiency and on the front surface of a 16.7% efficient truncated-pyramid MIS-IL cell. Furthermore, a 15.1% efficient standard MIS-IL cell as described elsewhere[31,45] was included. For this cell, the thermal oxide in the SiO/Cs/SiN passivation scheme was grown at 500°C. All cells were fabricated on 0.5- or 1.5-$\Omega \cdot$cm boron-doped FZ silicon wafers and use a 70-nm thick remote-plasma SiN film as combined passivation and antireflection layer. The UV test was performed with the same set-up as described above. To perform a realistic test for solar cells, a UV filter with a cut-off wavelength of 340 nm was used, representing the PV module encapsulation. For wavelengths between 340 and 400 nm, the average intensity of the UV lamp is seven times the intensity of the AM1.5G spectrum. (Note that photons with $\lambda > 400$ nm do not have any impact on the passivation quality of remote-plasma SiN-passivated emitters or p-type FZ substrates.) At several stages during the UV test the cell parameter efficiency η, fill factor FF, open-circuit voltage V_{oc} and short-circuit current density J_{sc} were measured at a light intensity of 100 mW cm^{-2} and a cell temperature of 25°C.

Figure 17 shows the measured cell parameters of a remote-plasma SiN-passivated diffused p-n junction Si solar cell during UV exposure, together with a schematic of the illuminated front surface design of the cell. In agreement with Ref. 34 we observe perfect stability of all cell parameters during 600 h of UV exposure, corresponding to about 4.3 years of outdoor operation in glass-encapsulated modules. Figure 18 shows the rear-illuminated cell parameters of a remote-plasma SiN-passivated bifacial p-n junction cell during UV exposure, together with a schematic of the illuminated rear surface of the cell. Perfect stability of all cell parameters is observed during the test. In typical bifacial applications the rear intensity of the PV module does not exceed 50% of the front intensity. Thus, our 600-h UV test corresponds to an outdoor operation of the cells of more than 8 years. These results confirm the previous conclusions (see discussion of Figure 9) that remote-plasma SiN films provide stable rear efficiencies of 17–18% of bifacial Si solar cells. It should be noted that in contrast to PCD samples solar cells possess metal contacts; hence, they are much less sensitive to changes in the SRV at the SiN-passivated surface areas than the previously described PCD samples. Figure 19 shows the cell parameters of both a standard MIS-IL cell and a truncated-pyramid MIS-IL cell during UV exposure, together with a schematic of the illuminated front surface design of the standard MIS-IL cell. As can be seen, all parameters of both cells are stable during the 600-h UV test, corresponding to an outdoor operation of the cells of about 4.3 years.

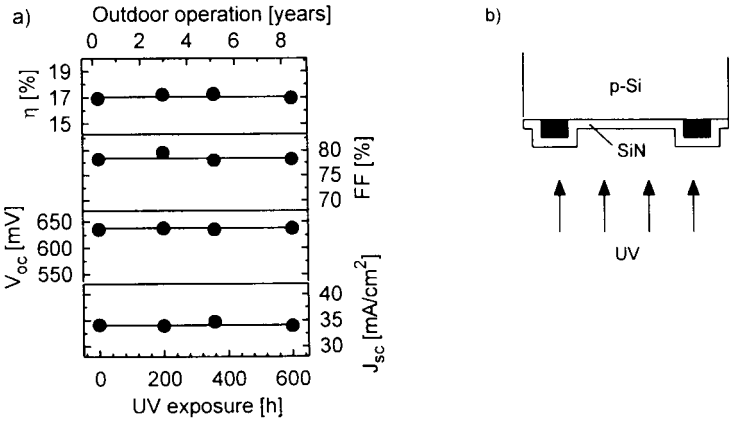

Figure 18. (a) Measured rear-illuminated cell parameters of a remote-plasma SiN-passivated bifacial p-n junction Si solar cell during UV exposure. The solid lines are first-order regressions. (b) Schematic of the illuminated rear surface design. The SiN film has a thickness of 70 nm

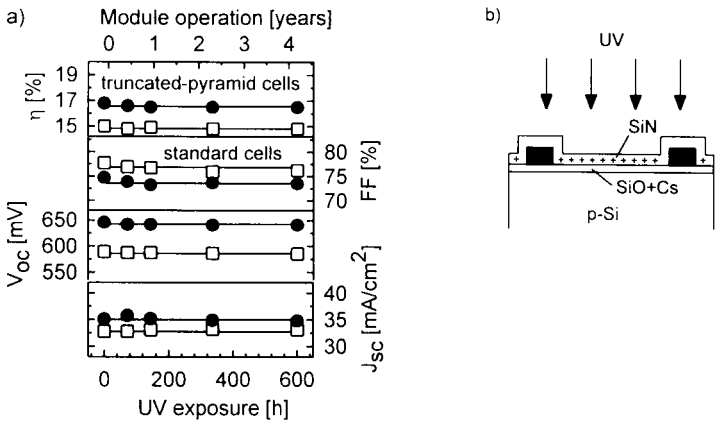

Figure 19. (a) Measured cell parameters of standard and truncated-pyramid MIS-IL silicon solar cells during UV exposure. The solid lines are first-order regressions. (b) Schematic of the illuminated front surface of the standard ('first-generation') MIS-IL cell

CONCLUSIONS

Fabrication of solar cells can be enormously simplified by means of low-temperature surface passivation. In this paper, significant progress in the area of low-temperature passivated crystalline Si solar cells fabricated on p-type substrates is reported. Using SiN films generated at 375°C in a remote PECVD system, we succeeded to achieve SRVs as low as 4 cm s^{-1} on polished 1.5-$\Omega \cdot$ cm FZ p-silicon wafers. This is by a clear margin the lowest SRV that has ever been obtained on a low-resistivity p-Si wafer passivated by a solid film, regardless of the complexity, the speed and the temperature of the film fabrication process. On phosphorus-diffused emitters fabricated on 1.5-$\Omega \cdot$ cm p-Si wafers, the plasma SiN films generate J_{oe} values of about 150 fA cm^{-2} at 300 K, which is comparable to the case of high-quality oxide passivation of our emitters. Even better emitter properties are obtained if the remote-plasma SiN films are combined with a thin thermal oxide and a CsCl dip in order to generate an induced-junction emitter.

Application of these remote-plasma SiN films to cost-effective Si solar cell designs presently under development at ISFH turned out to be most successful. In the area of diffused p-n junction cells, efficiencies above 19% were obtained. The excellent degree of surface passivation is further highlighted by

rear efficiencies above 18% for 'low-tech' bifacial Si solar cells, by far the highest ever reported for bifacial cells with non-diffused rear surfaces. The SiN films can also successfully be combined with a cost-effective mask-free metallization technique, as demonstrated by front efficiencies of 18.6% of shallow-angle evaporated p-n junction Si solar cells. In the area of inversion-layer cells, a combination of these SiN films with a thin thermal oxide and a CsCl dip allowed us to achieve 17.1% efficiency, which is a new record value for this inherently low-cost cell technology.

The efficiency of all investigated solar cells was stable during a 600-h UV test, corresponding to more than 4 years of glass-encapsulated outdoor operation. Hence, we are convinced that these cells would also be stable during the typical PV module lifetime of about 20 years. Using PCD samples as a much more sensitive test structure for the investigation of the UV stability of the surface passivation, a small degradation due to UV light is detectable at remote-plasma SiN-passivated p-Si surfaces corresponding to the non-metallized rear surface regions of bifacial cells. A detailed investigation of this phenomenon showed that the degradation becomes less pronounced with increasing SiN film thickness and with increasing photon wavelength. For wavelengths above 400 nm the remote-plasma SiN surface passivation is perfectly stable. The detected slight instability for wavelengths below 400 nm is too small to have any impact on the long-term stability of encapsulated 17–18% rear-efficient bifacial cells using this passivation scheme. It should be noted that this would not be the case for our present direct-plasma SiN films (either low-frequency or 13.56-MHz high-frequency excitation). Stable differential $S_{\mathrm{eff.d}}$ values of 23 cm s^{-1} on 1.5-$\Omega \cdot$ cm p-Si wafers are obtained with SiO/Cs/SiN passivation schemes as presently used on the front surface of our truncated-pyramid MIS-IL cells. This passivation scheme is also well suited for the rear surface of bifacial solar cells, giving the potential of stable rear efficiencies of silicon solar cells of even 20%. On the investigated n^+-diffused emitters, both direct-plasma and remote-plasma SiN films provide stable surface passivation.

The key result from this work is that, compared to thermal oxides grown at high temperature, low-temperature remote-plasma SiN films provide about equal surface passivation on phosphorus-diffused silicon surfaces and significantly superior surface passivation on low-resistivity p-Si wafers. Due to the low deposition temperatures ($\sim 375^{\circ}$C) and the high refraction index (~ 2.3), these SiN films act as highly efficient surface-passivating antireflection coatings. This unique combination offers great possibilities for significant cost reductions of PV electricity. Hence, we are presently working towards the realization of the above-mentioned cell concepts on large-area single- and multicrystalline p-Si wafers.

Acknowledgements

The authors would like to thank all members of the photovoltaic department at ISFH for their contributions to this work. The support by the State of Lower Saxony and the German Bundesministerium für Bildung, Wissenschaft, Forschung und Technologie is gratefully acknowledged. The ISFH is a member of the German Forschungsverbund Sonnenenergie.

REFERENCES

1. A. G. Aberle, S. J. Robinson, A. Wang, J. Zhao, S. R. Wenham and M. A. Green, 'High-efficiency silicon solar cells: fill factor limitations and non-ideal diode behaviour due to voltage-dependent rear surface recombination velocity', *Prog. Photovolt.*, **1**, 133 (1993).
2. R. Hezel, 'A new high efficiency solar cell concept based on truncated pyramids', *Conf. Rec. 1st World Conference on Photovoltaic Energy Conversion*, Hawaii, 1994, p. 1466.
3. R. Hezel, 'A novel approach to cost-effective high efficiency solar cells', *Conf. Rec. 13th European Photovoltaic Solar Energy Conference*, Nice, 1995, p. 115.
4. A. G. Aberle, S. Glunz and W. Warta, 'Impact of illumination level and oxide parameters on Shockley-Read-Hall recombination at the Si–SiO_2 interface', *J. Appl. Phys.*, **71**, 4422 (1992).
5. P. A. Basore, 'Numerical modeling of textured silicon solar cells using PC-1D', *IEEE Trans. Electron Devices*, **37**, 337 (1990).

6. A. Cuevas, P. A. Basore, G. Giroult-Matlakowski and C. Dubois, 'Surface recombination velocity and energy bandgap narrowing of highly doped n-type silicon', *Conf. Rec. 13th European Photovoltaic Solar Energy Conference*, Nice, 1995, p. 337.
7. R. R. King, R. A. Sinton and R. M. Swanson, 'Low surface recombination velocities on doped silicon and their implications for point contact solar cells', *Conf. Rec. 19th IEEE Photovoltaic Specialists Conference*, New Orleans, 1987, p. 1168.
8. A. Borghesi, B. Pivac, A. Sassella and A. Stella, 'Oxygen precipitation in silicon', *J. Appl. Phys.*, **77**, 4169 (1995).
9. S. R. Wenham, 'Buried-contact silicon solar cells', *Progr. Photovolt.*, **1**, 3 (1993).
10. A. G. Aberle, S. W. Glunz, A. W. Stephens and M. A. Green, 'High-efficiency silicon solar cells: Si–SiO_2 interface parameters and their impact on device performance', *Progr. Photovolt.*, **2**, 265 (1994).
11. A. G. Aberle, P. P. Altermatt, G. Heiser, S. J. Robinson, A. Wang, J. Zhao, U. Krumbein and M. A. Green, 'Limiting loss mechanisms in 23% efficient silicon solar cells', *J. Appl. Phys.*, **77**, 3491 (1995).
12. J. Zhao, A. Wang, P. P. Altermatt, S. R. Wenham and M. A. Green, '24% efficient silicon solar cells', *Conf. Rec. 1st World Conference on Photovoltaic Energy Conversion*, Hawaii, 1994, p. 1477.
13. P. E. Gruenbaum, R. A. Sinton and R. M. Swanson, 'Stability problems in point contact solar cells', *Conf. Rec. 20th IEEE Photovoltaic Specialists Conference*, Las Vegas, 1988, p. 423.
14. D. S. Ruby and W. K. Schubert, 'The effects of concentrated ultraviolet light on high-efficiency silicon solar cells', *Conf. Rec. 22nd IEEE Photovoltaic Specialists Conference*, Las Vegas, 1991, p. 111.
15. R. Hezel and R. Schörner, 'Plasma Si nitride — a promising dielectric to achieve high-quality silicon MIS/IL solar cells', *J. Appl. Phys.*, **52**, 3076 (1981).
16. R. Hezel, K. Blumenstock and R. Schörner, 'Interface states and fixed charges in MNOS structures with APCVD and plasma silicon nitride', *J. Electrochem. Soc.*, **131**, 1679 (1984).
17. A. G. Aberle, T. Lauinger, J. Schmidt and R. Hezel, 'Injection-level dependent surface recombination velocities at the silicon–plasma silicon nitride interface', *Appl. Phys. Lett.*, **66**, 2828 (1995).
18. C. Leguijt, 'Surface passivation for silicon solar cells', *PhD Thesis*, University of Utrecht, The Netherlands, 1995.
19. H. C. Neitzert, N. Layadi, P. Roca i Cabarrocas, R. Vanderhaghen and M. Kunst, '*In situ* measurements of changes in the structure and in the excess charge-carrier kinetics at the silicon surface during hydrogen and helium plasma exposure', *J. Appl. Phys.*, **78**, 1438 (1995).
20. T. Lauinger, J. Schmidt, A. G. Aberle and R. Hezel, 'Surface passivation properties of silicon/silicon oxide/silicon nitride structures for solar cells', *Conf. Rec. 13th European Photovoltaic Solar Energy Conference*, Nice, 1995, p. 1291.
21. G. Lucovsky and D. V. Tsu, 'Plasma enhanced chemical vapor deposition: differences between direct and remote plasma excitation', *J. Vac. Sci. Technol.*, **A5**, 2231 (1987).
22. J. Schmidt, T. Lauinger, A. G. Aberle and R. Hezel, 'Light-biased photoconductance decay measurements on silicon-nitride passivated silicon surfaces', *Conf. Rec. 13th European Photovoltaic Solar Energy Conference*, Nice, 1995, p. 1287.
23. T. Lauinger, J. Schmidt, A. G. Aberle and R. Hezel, 'Record low surface recombination velocities on 1 Ω cm p-silicon using remote plasma silicon nitride passivation', *Appl. Phys. Lett.*, **68**, 1232 (1996).
24. R. Brendel, 'Note on the interpretation of injection level dependent surface recombination velocities', *Appl. Phys. A*, **60**, 523 (1995).
25. A. G. Aberle, J. Schmidt and R. Brendel, 'On the data analysis of light-biased photoconductance decay measurements', *J. Appl. Phys.*, **79**, 1491 (1996).
26. J. Moschner, 'Optimierung und Charakterisierung von Plasmasiliciumnitridschichten zur Oberflächenpassivierung von Siliciumsolarzellen', *Diploma Thesis*, University of Hannover, Germany, 1996.
27. T. Lauinger, J. Moschner, A. G. Aberle and R. Hezel, 'Optimization and characterization of remote PECVD silicon nitride for the passivation of p-type crystalline silicon surfaces', Submitted to *J. Appl. Physics*, Jan. 1997.
28. J. Schmidt, T. Lauinger, A. G. Aberle and R. Hezel, 'Record low surface recombination velocities on low-resistivity silicon solar cell substrates', *Conf. Rec. 25th IEEE Photovoltaic Specialists Conference*, Washington, DC, 1996, p. 413.
29. A. W. Stephens, A. G. Aberle and M. A. Green, 'Surface recombination velocity measurements at the silicon-silicon dioxide interface by microwave-detected photoconductance decay', *J. Appl. Phys.*, **76**, 363 (1994).
30. S. W. Glunz, A. B. Sproul, W. Warta and W. Wettling, 'Injection level dependent recombination velocities at the Si–SiO_2 interface for various dopant concentrations', *J. Appl. Phys.*, **75**, 1611 (1994).
31. R. Hezel, W. Hoffmann and K. Jäger, 'Recent advances in silicon inversion layer solar cells and their transfer to industrial pilot production', *Conf. Rec. 10th European Photovoltaic Solar Energy Conference*, Lisbon, 1991, p. 511.

32. W. Bauch, K. Jäger and R. Hezel, 'Effect of Cs contamination on the interface state density of MNOS capacitors', *Appl. Surf. Sc.*, **39**, 356 (1989).
33. M. Grauvogl, A. G. Aberle and R. Hezel, '17.1% efficient truncated-pyramid inversion-layer silicon solar cells', *Conf. Rec. 25th IEEE Photovoltaic Specialists Conference*, Washington, DC, 1996, p. 433.
34. Z. Chen, A. Rohatgi and D. Ruby, 'Silicon surface and bulk defect passivation by low temperature PECVD oxides and nitrides', *Conf. Rec. 1st World Conference on Photovoltaic Energy Conversion*, Hawaii, 1994, p. 1331.
35. D. Ruby, W. L. Wilbanks and C. B. Fleddermann, 'A statistical analysis of the effect of PECVD deposition parameters on surface and bulk recombination in silicon solar cells', *Conf. Rec. 1st World Conference on Photo1voltaic Energy Conversion*, Hawaii, 1994, p. 1335.
36. A. G. Aberle and R. Hezel, 'Advances in low-temperature passivated silicon solar cells', *Conf. Rec. 25th IEEE Photovoltaic Specialists Conference*, Washington, DC, 1996, p. 371.
37. T. Lauinger, J. Moschner, A. G. Aberle and R. Hezel, 'UV stability of highest-quality plasma silicon nitride passivation of silicon solar cells', *Conf. Rec. 25th IEEE Photovoltaic Specialists Conference*, Washington, DC, 1996, p. 417.
38. T. Lauinger, B. Lenkeit, A. Hübner, A. G. Aberle and R. Hezel, unpublished results.
39. A. Hübner, A. G. Aberle and R. Hezel, 'Cost-effective bifacial silicon solar cells with 19% front and 18% rear efficiency', *Conf. Rec. 25th IEEE Photovoltaic Specialists Conference*, Washington, DC, 1996, p. 489.
40. R. Hezel and K. Jäger, 'Low-temperature surface passivation of silicon solar cells', *J. Electrochem. Soc.*, **136**, 518 (1989).
41. S. R. Wenham, S. Bowden, M. Dickinson, R. Largent, D. Jordan, C. B. Honsberg and M. A. Green, 'Prototype photovoltaic roof tiles', *Conf. Rec. 13th European Photovoltaic Solar Energy Conference*, Nice, 1995, p. 1483.
42. B. Mayregger, R. Auer, M. Niemann, A. G. Aberle and R. Hezel, 'Performance of a low-cost static concentrator with bifacial solar cells', *Conf. Rec. 13th European Photovoltaic Solar Energy Conference*, Nice, 1995, p. 2377.
43. T. Nordmann and A. Goetzberger, 'Motorway sound barriers: the bifacial north/south concept and the potential in Germany', *Conf. Rec. 13th European Photovoltaic Solar Energy Conference*, Nice, 1995, p. 707.
44. A. Cuevas, A. Luque, J. Eguren and J. Del Alamo, '50 per cent more output power from an albedo-collecting flat panel using bifacial solar cells', *Sol. Energy*, **29**, 419 (1982).
45. A. G. Aberle, B. Kuhlmann, R. Meyer, A. Hübner, C. Hampe and R. Hezel, 'Comparison of p-n junction and inversion-layer silicon solar cells by means of experiment and simulation', *Progr. Photovolt.*, **4**, 193 (1996).
46. M. Verbeek, A. Metz, A. G. Aberle and R. Hezel, 'Mechanically grooved high-efficiency silicon solar cells with self-aligned metallization', *Conf. Rec. 25th IEEE Photovoltaic Specialists Conference*, Washington, DC, 1996, p. 521.
47. K. Jäger-Hezel, W. Schmidt, W. Heit and K. D. Rasch, 'Improved large area MIS-contacted silicon solar cells', *Conf. Rec. 13th European Photovoltaic Solar Energy Conference*, Nice, 1995, p. 1515.
48. *ISE PV-Charts*, 7th Edn, Fraunhofer Institute FhG-ISE, Freiburg, Germany, 1996.

